Understanding chromatic aberration impacts on lithographic imaging

Kafai Lai
IBM Microelectronics
Semiconductor Research and Development Center
East Fishkill, New York
E-mail: kafailai@us.ibm.com

Ivan Lalovic*
Cymer Inc.
San Diego, California

Bob Fair
IBM Microelectronics
Semiconductor Research and Development Center
East Fishkill, New York

Armen Kroyan†
Cymer Inc.
San Diego, California

Christopher J. Progler‡
IBM Microelectronics
Semiconductor Research and Development Center
East Fishkill, New York

Nigel Farrar
Cymer Inc.
San Diego, California

Dennis Ames
IBM Microelectronics
Semiconductor Research and Development Center
East Fishkill, New York

Khurshid Ahmed
Cymer Inc.
San Diego, California

Abstract. Recent development of high-precision aberration measurement techniques has enabled *in situ* characterization of the aberration response to wavelength offset. These measurements show that majority of the reconstructed Zernike terms exhibit some degree of sensitivity to wavelength. Although this dependence diminishes with the increasing order of Zernike polynomial, we consider the cumulative contribution of five Zernike terms, which have the strongest wavelength dependence (*Z2*, *Z4*, *Z6*, *Z8*, *and Z11*). The imaging impacts of KrF laser wavelength and spectral bandwidth are investigated using aerial image simulation; the behavior of the process window, mask error enhancement factor (MEEF), image placement, proximity effect, and sidelobe intensity is quantified. In this model, the chromatic aberrations are experimentally measured in a 0.68-NA KrF step-and-scan exposure system using the LITEL aberration test (InspecStep interferometer manufactured by LITEL Instruments, Inc., San Diego, California). The illumination spectrum input is characterized by spectroscopic measurement of a 2-KHz KrF laser source. In the lithography model, it is important to incorporate all of the wavelength-sensitive terms due to the additive contribution to the overall lens aberration balance. As shown previously, the longitudinal and lateral chromatic aberrations (image height and magnification) are the most sensitive to shift in center wavelength and have the strongest contribution to the aerial image modulation. Simulation results show several imaging changes for isolated lines and contact holes with changes in illumination spectrum. However, the rates of change are shown to decrease as bandwidth is reduced well into the subpicometer level. In the case of isolated contacts, the depth of focus (DOF) increases with the increase in bandwidth, however, at the expense of reduced exposure latitude. This suggests that engineering the spectral output of the laser can provide some process enhancement, although careful compromise is needed to utilize any DOF enhancement, since other image metrics including MEEF, side-lobe intensity, and image placement are also affected. *© 2003 Society of Photo-Optical Instrumentation Engineers.*
[DOI: 10.1117/1.1562929]

Subject terms: chromatic aberration; excimer lasers; lithography.

Paper 01027 received Nov. 2, 2001; revised manuscript received Oct. 14, 2002; accepted for publication Nov. 4, 2002.

1 Introduction

In pursuit of low k1 optical lithography, the performance of every subsystem of an exposure tool needs to be optimized. In particular this pertains to modules affecting projection imaging, such as lens aberrations, scan synchronization, dose control, overlay, illumination power, and partial coherence uniformity. System optimization is important since it reduces the tool-induced error contribution to the overall error budget, enabling manufacturability under stringent process latitude conditions.

The performance and optimization of the excimer laser source also has implications on image quality. In the deep UV (DUV), silicon dioxide (SiO_2) and calcium fluoride (CaF_2) exhibit significant dispersion resulting in changes in the image plane position as well as the ray-geometric aberration balance. Since the dispersion of the two available lens materials cannot be counteracted, industry-wide adoption of line-narrowed excimer lasers has been required for high-throughput DUV projection exposure systems. However, even the half-picometer illumination spectra of the line-narrowed excimer laser source have been shown to interact with lithographic image formation using experiment[1] and simulation.[2] In these studies, the key components are understanding the illumination spectrum of the laser source and the aberration-wavelength (chromatic) lens response. The interaction of these two parameters modulates the out-

*Present address: Advanced Micro Devices, One AMD Place, P.O. Box 3453, MS78, Sunnyvale, California 94088-3453.
†Present address: Numerical Technologies, San Jose, California.
‡Present address: Photronics, Dallas, Texas.

 © 2003 Society of Photo-Optical Instrumentation Engineers

put aerial image and governs the magnitude of the response. The interaction mechanism is described in the following sections.

The majority of lithography simulation done today assumes monochromatic illumination and a constant lens aberration value; therefore typically the chromatic lens response is unaccounted for. Although, this is a useful simplification, which may lead to faster computation, it is not an accurate description of the entire imaging process in practice. The spectral extent of excimer laser systems is indeed quite narrow (0.5 to 0.6 pm full-width-at-half-maximum for the system studied), however it is not monochromatic; i.e., the bandwidth has a nonzero physical extent and the shape of the spectrum, including the background intensity, is of importance.[3] Furthermore, the center wavelength of the KrF source is tunable over an extended range spanning several tens of nanometers.

In this work, we use aerial image simulation to quantify the effects of the center wavelength offset and bandwidth changes of the KrF laser on imaging of isolated lines and contact holes. Here, we present and analyze the results for 150-nm isolated lines and 150-nm contacts in order to show that variation of the laser bandwidth can produce diverging results as a function of the feature geometry. Similarly, selection of photoresist process conditions and illumination condition contributes to varied bandwidth-induced responses. The simulations are based on experimentally obtained lens chromatic aberration input, evaluated in a 0.68-NA DUV step-and-scan system, and in addition, high-precision spectroscopic measurements of a production 2-kHz KrF excimer laser. Changes of the lens chromatic aberrations (as a function of different lens designs, NA, materials) also lead to a varied image-bandwidth response.

2 Experiment and Modeling

2.1 *Aberration Measurement*

The lens chromatic aberrations were quantified for a 248-nm step-and-scan exposure system with 0.68 NA using the LITEL aberration measurement method.[4,5] The dependency of the 28 Zernike coefficients to change in the center wavelength of the laser is analyzed at ten points along the center of the slit in the slit direction (x-direction). The wafer exposures are done in static mode, with several fields exposed under the same wavelength setting for redundancy. In addition to the nominal wavelength (248.3225 nm), the following eight wavelength conditions were tested: $+/-9$ pm, $+/-4$ pm, $+/-1$ pm, and $+/-0.4$ pm (offset from nominal). The wavelength was varied using software control of the line narrowing module accessed through the laser interface keypad (paddle). The illumination condition of the projection exposure system was set to the maximum lens NA of 0.68 NA and 0.75σ (partial coherence). The wafer measurement of the photoresist aberration diagnostic patterns was done using a high-accuracy optical overlay microscope.

The change in Zernike coefficients as a function of wavelength offset are shown in Fig. 1, for a given field point at one side $(-x)$ of the static field (slit). The aberration data for each wavelength setting is subtracted from the nominal lens fingerprint to show the absolute changes in the Zernike coefficients, expressed in waves (1wave

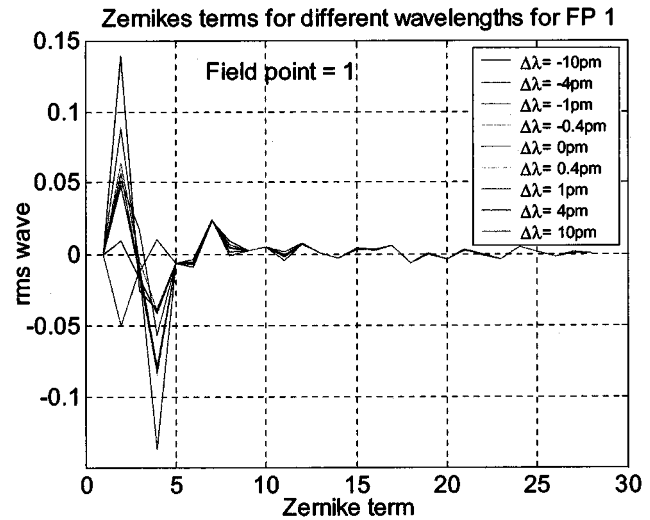

Fig. 1 Plot of Zernike coefficients (Noll's ordering) for different center wavelengths. The Zernike coefficients are constant except for A2, A4, A6, A8, and A11 (wavefront tilt, defocus, astigmatism, coma, and spherical aberration, respectively).

$\sim$248 nm). We see that the low-order terms Z2 (x-tilt) and Z4 (focus) are most strongly affected by wavelength offset. Z3 (y-tilt) is expected to have a response similar to Z2, however, since the sampling point is located near the center of the slit $(y=0)$ no magnification effect is observed.

Figure 2 shows the surface responses of the terms that appreciably vary with wavelength (Z2, x-tilt; Z4, focus; Z6,

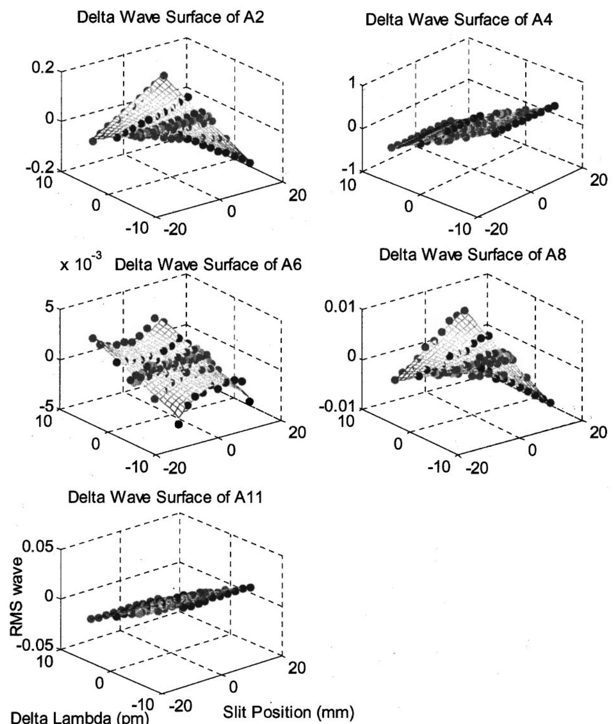

Fig. 2 Chromatic aberration model showing Zernike terms that are affected and their dependence on center wavelength and slit position (A2 = tilt, A4 = focus, A6 = xy-Astigmatism, A8 = x-coma, A11 = spherical aberration).

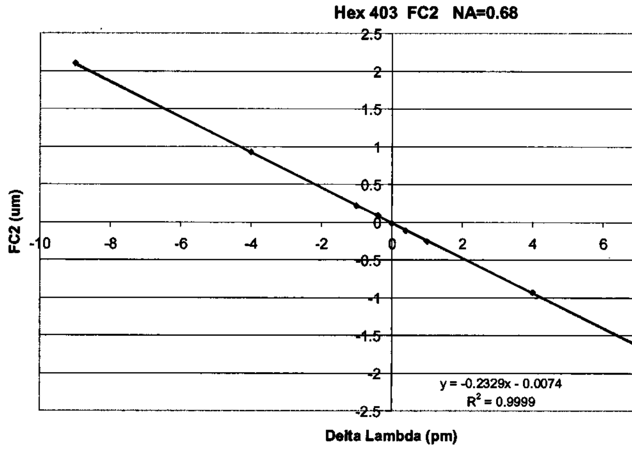

Fig. 3 *In situ* focus measurement for different center wavelengths. A linear response of defocus is observed for a change in λ0. FC2 is the focus reading in microns from this test.

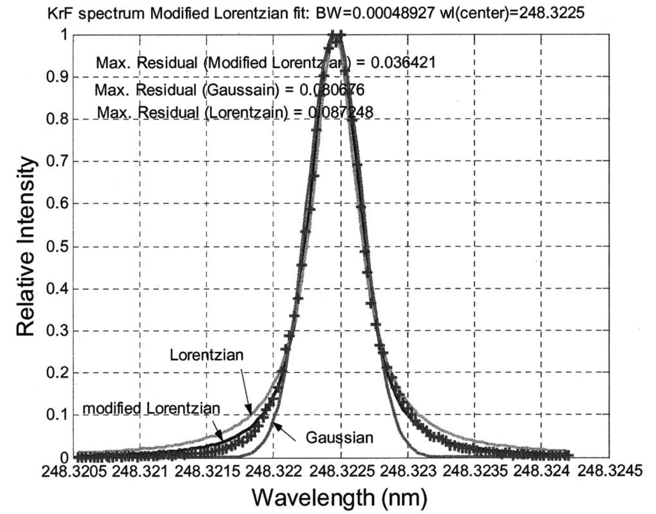

Fig. 4 The measured KrF spectrum and various fitting models. The modified Lorentzian fit the spectrum better.

x/y-astigmatism; Z8, primary coma; and Z11, primary spherical). Some of the terms exhibit varied response depending on slit position (in the x-direction, along the slit). For example, we observe a linear lateral magnification error from wavefront tilt (Z2) and a nonlinear lateral magnification from coma (Z8). On the other hand, the linear focus (Z4)-wavelength response is largely independent of slit position. The least-squares slope of the focus-wavelength slope is $\sim 0.233\ \mu$m/pm (or 233 nm/pm), with an R^2 value approaching unity. This result, for the longitudinal chromatic aberration, is in good agreement with results previously published for comparable systems.[1,2] The result of the Litel measurements are confirmed by an *in situ* sensor-based focus measurement in the exposure system as shown in Fig. 3. The least-squares fit for the longitudinal chromatic aberration results of the Litel and the focus-sensor results are in excellent agreement (within 0.05%).

Below is the list of the fitted wavelength responses of the given Zernike coefficients $A_N(\lambda,h)$, where dA denotes the coefficient change in waves and N is the polynomial order:

$$dA_2 = 9.06E-4*h*d\lambda - 1.67E-5*d\lambda,$$

$$dA_4 = -7.1901E-2*d\lambda,$$

$$dA_6 = 1.73E-6*h^2*d\lambda - 5.81E-7*d\lambda,$$

$$dA_8 = 5.30E-5*h*d\lambda - 4.07E-6*d\lambda,$$

$$dA_{11} = -2.854E-3*d\lambda.$$

Here h represents the field height in millimeters and $d\lambda$ represents wavelength change in nanometers. The polynomial surface fits are truncated at the second order. We observe that defocus and magnification errors, from this formalism, exhibit the most significant chromatic sensitivity.

2.2 *Laser Spectrum Modeling*

As an input to simulation, a high-accuracy spectroscopic measurement of a 2-kHz KrF excimer laser system is used. Although using raw spectrum data may be preferential and has been used in previous work, in this study the raw data is fitted in order to allow resampling of the spectrum, enabling direct control over the computation time. In this work, the raw spectrum is fitted using a modified Lorentzian function,[6] which can be written in the following functional form:

$$g(\lambda) = (\Delta\lambda)^n / \{[2(\lambda - \lambda_0)]^n + \Delta\lambda^n\},$$

where $g(\lambda)$ is the output intensity at a wavelength λ, $\Delta\lambda$ is the full-width-at-half-maximum (FWHM) bandwidth, λ_0 is the center wavelength, and n is the free-fitting parameter. The spectrum $g(\lambda)$ is normalized to 1 at $\lambda = \lambda_0$ and therefore $g(\lambda) = \frac{1}{2}$, when $\lambda - \lambda_0 = \Delta\lambda/2$, corresponding to the FWHM level.

The measured and fitted spectra are shown in Fig. 4. In this figure, we see that the raw data points are described better by the modified Lorentzian than either a true Lorentzian or Gaussian function. The maximum residual for the modified Lorentzian is approximately 0.08 for the given measured spectrum with 0.49-pm FWHM bandwidth. It is important to fit the spectrum as accurately as possible, particularly in the tails of the spectrum, since the image contrast is very sensitive to the energy in these regions. In this simulation, modification of the bandwidth is done by rescaling the domain, therefore adjustment of the $\Delta\lambda$, FWHM parameter. The modeled spectral bandwidth is modified from 0 pm (monochromatic) to 2 pm FWHM. It should be noted that both extremes are well outside the typical design and operating range of current line-narrowed systems, which is between 0.4 and 0.6 pm.

2.3 *Polychromatic Lithography Modeling*

The impact of laser wavelength and bandwidth on imaging is simulated using PROLITH/2.[7] The aerial image contribution of each wavelength component is assumed to be purely additive, therefore assuming incoherent light interaction at the image plane, as discussed in Ref. 2. The polychromatic aerial image is therefore given by a weighted

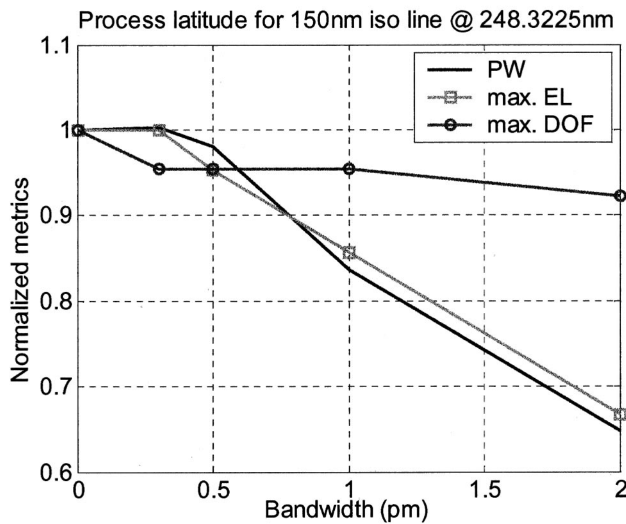

Fig. 5 The degradation of process window for increase of bandwidth for 150-nm isolated lines. The NA used is 0.68 and sigma is 0.75-0.5 annular.

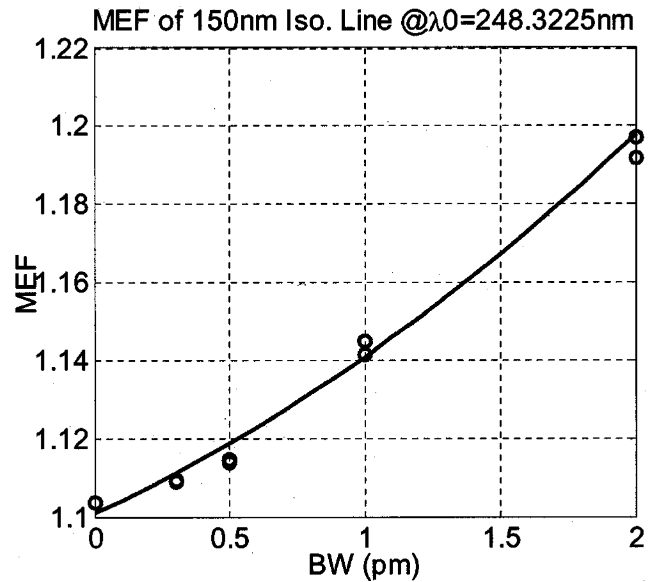

Fig. 6 The MEEF degradation with bandwidth (BW) for a 150-nm isolated line. For each bandwidth, the MEEF for vertical and horizontal features are plotted. The solid line is a fitted quadratic curve. The illumination is 0.75-0.5 annular.

superposition of all of the individually computed aerial images corresponding to different wavelength components. The image superposition is weighted by the laser spectrum, $g(\lambda)$. Each individually computed aerial image, corresponding to a given wavelength component, is assigned a single Zernike polynomial set given by the chromatic aberration model, $A_N(\lambda,h)$.

It should be noted that the results derived here apply to a specific exposure system, for which the lens aberrations and laser spectrum were measured. Although these characteristics will depend on lens design, the qualitative effect of laser wavelength and bandwidth on process performance should be generally applicable to all DUV lens designs.

3 Results and Discussions

3.1 *Lithographic Simulation*

In this study, isolated lines and isolated contact holes are simulated using 0.68-NA projection and annular illumination of 0.75/0.5, optimized for imaging of these features. Based on the aerial image response alone, the integrated process window [DOF and exposure latitude (EL)], image placement, mask error enhancement factor (MEEF), and through-pitch CD characteristics are quantified as a function of spectral width. In addition, the aerial image sidelobe to main lobe intensity ratio is simulated for packed contact holes projected using attenuated phase shift mask (att-PSM).

3.1.1 *150-nm isolated lines*

For the 150-nm isolated line, as shown in Fig. 5, the process window (PW) area, including DOF and EL, is reduced with increasing bandwidth. In Fig. 5, the PW, EL, and DOF results are normalized to 1 at the monochromatic $\Delta\lambda=0$ pm condition. The change of the PW parameters is nonlinear in nature. In fact, the process window area change is less than 2.5% for bandwidth under 0.5 pm FWHM. For bandwidth above 0.6 pm, the process window reduction becomes more noticeable due to the diminishing exposure latitude. Interestingly, the DOF appears largely insensitive to bandwidth, showing only an 8% reduction at the 2-pm FWHM level, which is consistent with previously published results.

For this feature geometry, the resulting change in MEEF is relatively linear with a slope of approximately +4.7% per 1 pm of FWHM as shown in Fig. 6. Image placement was also quantified for this geometry, and although it exhibits sensitivity to wavelength offset, a negligible effect is caused by change in bandwidth. A magnification error of 0.62 nm/mm/pm is calculated as a function of wavelength offset, shown in Fig. 7. In Fig. 8 for the 150-nm lines, changes in optical proximity effect are also observed with increasing bandwidth as a function of pitch. Here, also the change in proximity bias is nonlinear with change in bandwidth. The change of the iso-dense bias as a function of FWHM bandwidth is shown in Fig. 9. The increasing sensitivity in the change of linewidth for broader bandwidths is due to the typically nonlinear dependence of linewidth on image defocus, and contrast loss, caused by components of the spectrum further from the central wavelength. Since this dependence is more sensitive for isolated lines, compared to dense lines, the proximity bias also shows a nonlinear dependence on bandwidth.

3.1.2 *150-nm isolated att-PSM contact holes*

The process window is also calculated for 150-nm isolated contact holes. The feature is imaged using an attenuated phase-shift structure using optimized 0.68-NA projection and annular illumination of 0.75/0.5. In Fig. 10, we observe process window behavior that is different than for isolated lines. Specifically, for bandwidths above 0.5 pm FWHM, a gradual increase of DOF is observed with bandwidth, which continues to the 2-pm FWHM level. At the same time, reduction of the EL is also apparent; the magnitude of

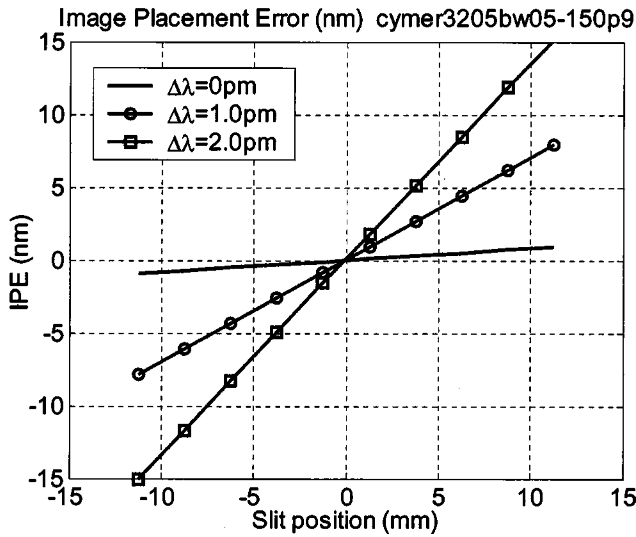

Fig. 7 Image displacement across slit for different center wavelength shift (Δλ) for a 150-nm isolated line. The linear behavior implies a magnification error. The slight tilt for zero wavelength shift is due to residue magnification on the system.

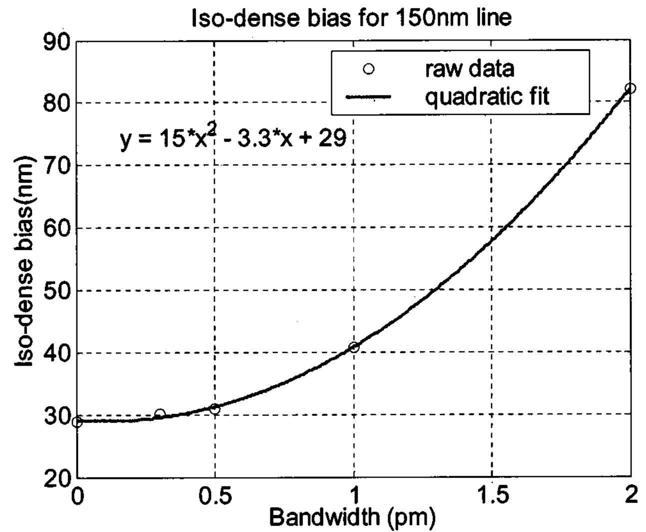

Fig. 9 Iso-dense bias for 150-nm line with various bandwidth. The data is derived from Fig. 8.

the EL reduction in this case is similar to that of 150-nm isolated lines. The cumulative effect of the DOF increase and EL reduction causes the total window to remain relatively constant (within 10% of nominal) for FWHM bandwidths up to 2 pm.

For the same features (150-nm att-PSM contacts) the bandwidth increase results in a MEEF increase of 14.7% per 1 pm FWHM as shown in Fig. 11. This is more than three times the change in MEEF of 150-nm isolated lines. Also for this geometry, the magnification error as a function of wavelength (0.71 nm/mm/pm) is approximately 14.5% larger than for isolated lines, shown in Fig. 12.

In addition we calculate the intensity ratio between the peak of the aerial image side lobe to the intensity peak of the main lobe. This result is shown in Fig. 13 and shows relatively linear increase in the side-to-main lobe ratio over our bandwidth domain. Least squares fit yields the change of side-to-main lobe ratio of $+0.031$/pm FWHM ($R^2 = 0.99$). The change of the ratio is approximately quadratic with wavelength offset due to the dominating defocus term, $A_4(\lambda)$. The wavelength dependence is shown in Fig. 14.

Due to the varying magnitude of the effect of bandwidth change on PW (EL and DOF), MEEF, and image placement, a careful compromise in process consideration is needed to utilize any appreciable DOF enhancement in a process application.

4 Conclusion

In conclusion, changes of the Zernike coefficients related to chromatic aberration were characterized on a state-of-the-art KrF scanner. The aberration response and experimentally measured laser spectrum were used to construct an aerial image model. Analysis of multiple lithographic pa-

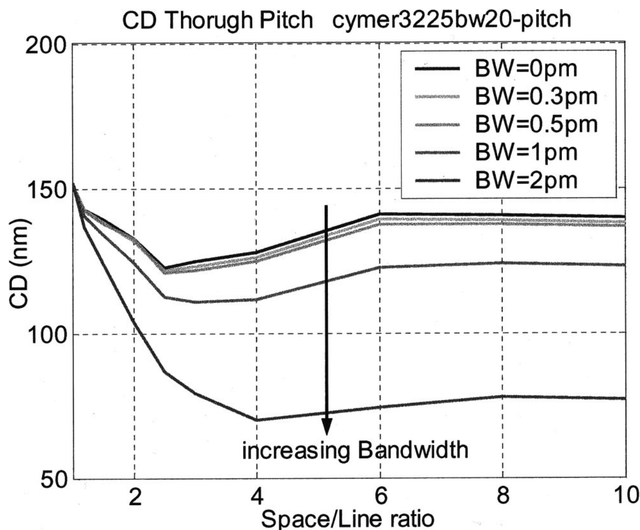

Fig. 8 CD through pitch curves for different bandwidths for a 150-nm line. The NA used is 0.68 and sigma is 0.75-0.5 annular.

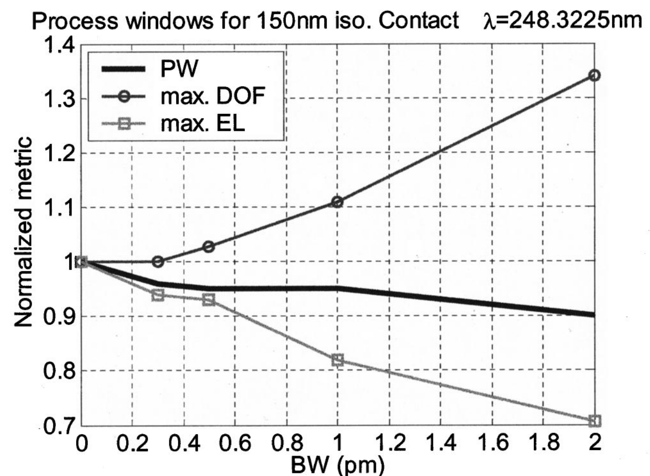

Fig. 10 Degradation of process window for increase of bandwidth (BW) for 150-nm isolated contact. The NA used is 0.68 and sigma is 0.75-0.5 annular.

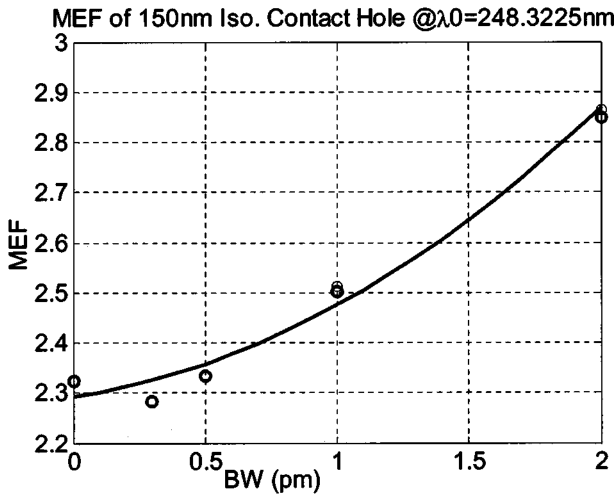

Fig. 11 The MEEF degradation with bandwidth for 150-nm contact. The two data points per each bandwidth correspond to horizontal and vertical features. The solid line is a quadratic fit to the data. The NA used is 0.68 and sigma is 0.75-0.5 annular.

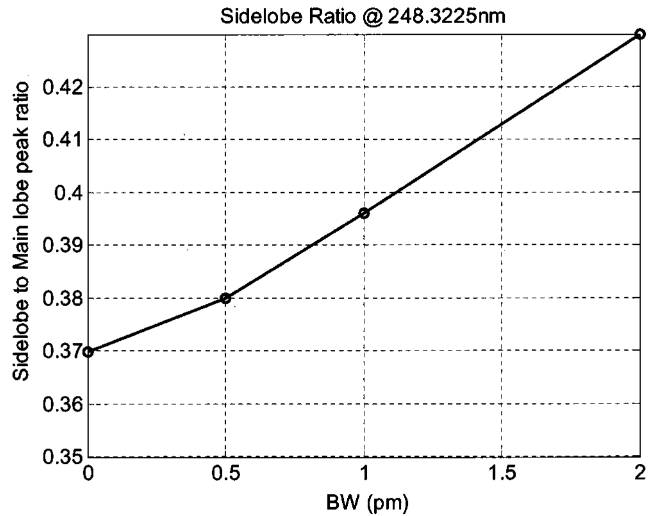

Fig. 13 Sidelobe to main lobe intensity ratio change with bandwidth change for 150-nm isolated contact.

rameters such as process window, MEEF, magnification error, and side-to-main lobe intensity ratio (for contact holes) was carried out to evaluate the effects of the excimer laser source bandwidth.

The process window simulation results for the worst case scenario here (isolated contact-hole EL) show a diminishing benefit of reducing the FWHM bandwidth past a given threshold. For 150-nm contacts, the EL does not change significantly from 0.5 to 0.3 pm. Compared to the monochromatic case, approximately 6% EL reduction is obtained with 0.5 pm and 5% EL reduction at 0.3 pm FWHM. The use of spectral broadening to enhance the DOF of isolated contact holes requires careful process tradeoff and optimization of PW, MEEF, image placements, and sidewall photoresist profile as well as all other critical process effects. The effect of such laser spectral engineering is similar to past work on adjusting the image focal plane during exposure, such as Hitachi's FLEX[8] technique or scanning using an image field tilted in the scan direction. However, these techniques are less flexible than laser spectral modification, which in principle allows a continuous range of adjustment necessary for process optimization.

The difference in results for isolated lines and isolated contacts suggests that all of the critical process parameters and their interactions need to be understood to evaluate the impact of the laser spectral bandwidth. Following such characterization, the laser bandwidth and wavelength control requirements can be derived from the most limiting process responses. Our results indicate that there is a diminishing change in the process performance by reducing the bandwidth beyond the 0.5-pm level. However, the lower bandwidth limit is indeed dependent on the magnitude of chromatic aberrations, illumination condition (off-axis illumination and/or PSM), and the critical feature geometry.

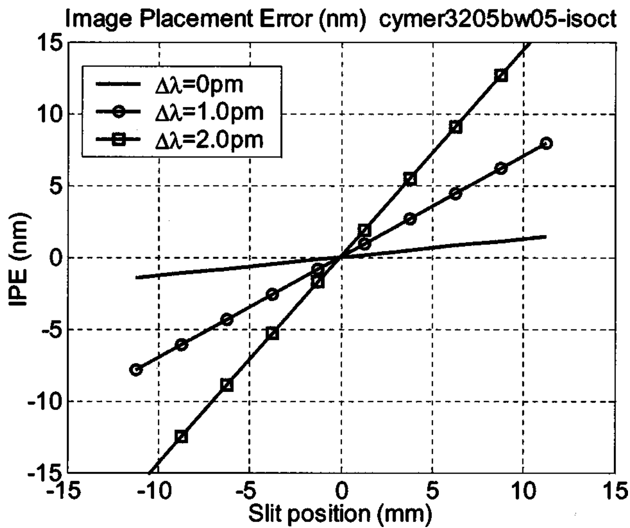

Fig. 12 The image displacement across slit for different center wavelength shift (Δλ) for 150-nm isolated contact. Note the magnification error is slightly higher than the 150-nm iso. line.

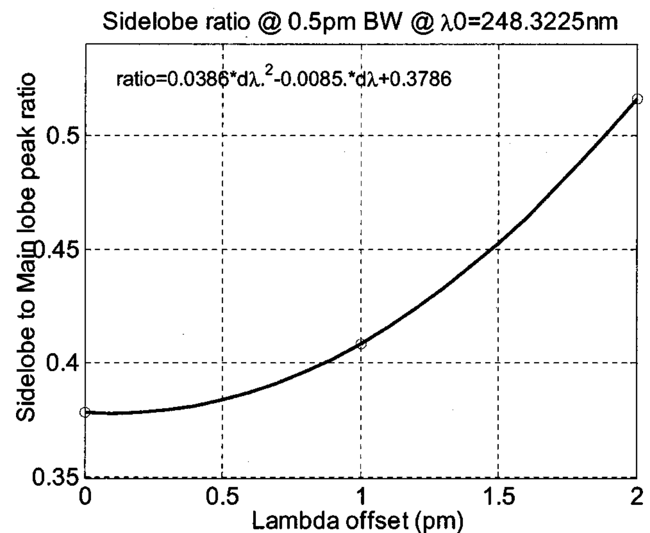

Fig. 14 Sidelobe to main lobe intensity ratio change with center wavelength for 150-nm isolated contact.

Exposure systems and lithographic processes with higher numerical apertures continued development in the area of excimer laser line narrowing. In addition to understanding the absolute bandwidth limits, flexible tuning of the center wavelength and bandwidth of the excimer laser would allow the selection of an optimal operating point from the standpoint of either process optimization or system performance efficiency.

Acknowledgments

The authors would like to thank Scott Schank for his experimental support, and Carlos Fonseca for his simulation software support. Both are from the SRDC of IBM. The assistance of Ben White, Cymer Field Service, is also recognized.

References

1. I. Lalovic et al., "Effects on illumination spectral width on mask error enhancement factor and iso-dense bias in 0.6NA KrF imaging," *Proc. SPIE* **4562**, 992–999 (2002).
2. A. Kroyan et al., "Modeling the effects of excimer laser bandwidths on lithographic performance," *Proc. SPIE* **4000**, 658–664 (2000).
3. A. Kroyan et al., "Effects of E95% integral vs. FWHM bandwidth specifications on lithographic imaging," *Proc. SPIE* **4346**, 1244–1253 (2001).
4. InspecStep interferometer manufactured by LITEL Instruments, Inc., San Diego, CA.
5. A. H. Smith et al., "Apparatus, method of measurement and method of data analysis for correction of optical system," U.S. patent No. 5,828,455 (1998).
6. R. Sandstrom, Cymer Inc., Private communication (2000).
7. PROLITH/2 is a registered trademark of KLA-Tencor, San Jose, CA.
8. H. Fukuda et al., "Improvement of defocus tolerance in a half-micron optical lithography by the focus latitude enhancement exposure method: Simulation and experiment," *J. Vac. Sci. Technol. B* **7**(4), 667–674 (1989).

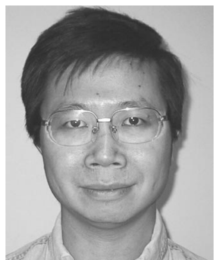

Kafai Lai received his BS in electrical engineering from the University of Hong Kong in 1988, and his MS and PhD degree in electrical engineering from the University of Texas at Austin in 1992 and 1995, respectively. He then joined Rockwell Semiconductor and Texas Instruments, working on lithography development. He currently works in the Semiconductor Research and Development Center at IBM Microelectronics focusing on optical imaging modeling and lens characterization.

Ivan Lalovic works on development and technology integration of 157-nm lithography at Advanced Micro Devices. His interests are directed toward imaging performance characterization and specification of advanced exposure systems, photomasks, and optical materials. Prior to joining AMD, Ivan worked as a lithography applications project manager at Cymer, Inc., developing the applications and technology roadmap requirements for KrF, ArF, and F2 excimer lithography. Ivan also worked at Hewlett-Packard Co. in lithography process development, transfer, and module integration. He obtained his BS in physics and MS in electrical engineering at the University of Washington.

Christopher J. Progler is currently corporate chief scientist with Photronics, a global manufacturer and integrator of photomasks. He graduated with a BS/MS in optics from the University of Rochester and received his PhD in electrical engineering from the University of Texas. In 2000 and 2001, he served as conference chair and proceeding editor for the SPIE Conference on Optical Microlithography. He also helped launch and is current chair of the SPIE Symposium on Advanced Microelectronic Manufacturing. Dr. Progler is associate editor for the SPIE *Journal of Microlithography, Microfabrication, and Microsystems*. Dr. Progler has published over 60 papers relating to advanced imaging sciences that have included numerous invited talks. He also holds multiple patents in lithography and received a high value patent award from IBM in 2001. Dr. Progler participates in a number of industry and consortia based advisory boards and working groups serving the semiconductor community.

Biographies and photographs of other authors not available.